Electrochimica Acta 127 (2014) 252–258

Contents lists available at ScienceDirect

Electrochimica Acta

journal homepage: www.elsevier.com/locate/electacta

Novel mesoporous silicon nanorod as an anode material for lithium ion batteries

Yanli Zhou [a], Xiaolei Jiang [a], Liang Chen [a], Jie Yue [a], Huayun Xu [a,*], Jian Yang [a,*], Yitai Qian [b]

[a] Key Laboratory of Colloid and Interface Chemistry, Ministry of Education School of Chemistry and Chemical Engineering, Shandong University, Jinan, 250100, P.R, China

[b] Hefei National Laboratory for Physical Science at Microscale, Department of Chemistry, University of Science and Technology of China, Hefei, 230026, P.R, China

ARTICLE INFO

Article history:
Received 13 November 2013
Received in revised form
19 December 2013
Accepted 30 January 2014
Available online 12 February 2014

Keywords:
Magnesiothermic reduction
Mesoporous silicon nanorods
Anode materials
Lithium ion batteries

ABSTRACT

Mesoporous silicon nanorods assembled by small nanocrystals were successfully prepared using multi-walled carbon nanotubes (MWCNTs) as a template via a facile magnesiothermic reduction process. The obtained product was characterized by X-ray diffraction, Raman spectroscopy, transmission electron microscopy, nitrogen adsorption-desorption measurement and electrochemical measurements. The resulting mesoporous silicon nanorods as an anode exhibit a significantly improved electrochemical performance compared with the porous silicon networks and bulk silicon. The reversible capacity can retain 1038 mAh g^{-1} at 200 mA g^{-1} after 170 cycles. Even at a high rate of 2000 mA g^{-1}, a reversible capacity of 664 mAh g^{-1} can still be obtained. All these results suggest that the mesoporous silicon nanorods are a promising candidate for the next generation of lithium ion batteries.

1. Introduction

Rechargeable lithium ion batteries (LIBs) as one of the most promising energy storage systems, have been successfully applied in portable electronic devices, hybrid electric vehicles (HEVs) and full electric vehicles (EVs) [1,2], due to their high energy density, high rate capability, light weight and long cycle life. Compared to the conventional graphite anode, silicon has many advantages, such as its high theoretical capacity (4200 mAh g^{-1}), low working potential, abundant and environmentally benign nature [3,4]. However, a large volume change (>300%) during the discharge and charge processes could lead to severe pulverization, cracking, and then a rapid capacity fading [3]. In order to address these issues, various nanostructures have been reported to alleviate the volume changes and improve the electrochemical properties of Si anodes during the discharge and charge processes. These nanostructures include nanowires [5,6], nanofilms [7–9], hollow nanospheres [10–12], and nanotubes [13,14].

Among these structures, one-dimensional nanomaterials have their own advantages as an anode for LIBs. First, one-dimensional nanomaterials can effectively accommodate the large volume changes and avoid the structure destruction [15]. Second, they can facilitate the electron transport inside the electrode [16]. A typical example is the application of Si nanowires as anode materials for LIBs synthesized by chemical-vapor-deposition (CVD) method [4,17,18].

Recently, magnesiothermic reduction has been considered as an eco-friendly, low-cost and facile route to synthesize Si nanomaterials [19–24]. Yang et al. synthesized a novel lotus-root-like mesoporous Si nanostructure using SBA-15 silica as a template, which showed a reversible capacity of 1500 mAh g^{-1} after 100 cycles at 1 C after surface carbon coating by a CVD process [21]. More recently, Yang et al. have reported the mesoporous silicon nanowires prepared by this method using poly-pyrrole (ppy) as a template, and the reversible capacities of 1826.8 and 737.4 mAh g^{-1} can be obtained at 500 mA g^{-1} and 10 A g^{-1} [24].

Herein, novel mesoporous Si nanorods were prepared using MWCNTs as a template via a facile magnesiothermic reduction method. The obtained product was characterized by X-ray diffraction, Raman spectroscopy, transmission electron microscopy, and nitrogen adsorption isotherm. When the mesoporous Si nanorods are used as an anode for LIBs, they display a better electrochemical performance than porous silicon networks and bulk silicon. We believe that the environmentally friendly and facile methods as well as the superior electrochemical performance make the mesoporous Si nanorods promising as anode materials for LIBs.

* Corresponding authors. Tel.: +86 0531 8836 4489, fax: +86 0531 8836 4489.
E-mail addresses: xuhuayun@sdu.edu.cn (H. Xu), yangjian@sdu.edu.cn (J. Yang).

http://dx.doi.org/10.1016/j.electacta.2014.01.158
0013-4686/

2. Experimental

2.1. Preparation of mesoporous Si nanorods

Pristine multi-walled carbon nanotubes (MWCNTs, China Shenzhen Nanotech Port Co., Ltd.) were treated with concentrated nitric acid as described previously [25].Then the composite of MWCNT/silica (SiO_2) was obtained according to the literature [26,27]. The composite was collected by centrifugation, washed with ethanol and deionized water, and dried at 60 °C for 5 h. After that, the MWCNT/SiO_2 composite was annealed at 700 °C for 8 h in air to remove the MWCNTs to obtain silica nanotubes. Subsequently, a mixture (mole ratio 2.5: 1) of SiO_2 nanotubes and magnesium (100-200 mesh, Sinopharm Chemical Reagent Co., Ltd.) was placed into a tube furnace, heated to 670 °C and held for 5 h in an Ar/H_2 atmosphere. The as-obtained product was treated with diluted hydrochloric acid (0.5 M), washed with water, and dried in a vacuum oven at 80 °C for 5 h to obtain the as-prepared brownish yellow mesoporous Si nanorods. The porous Si networks were also prepared by a similar process by doubling the amount of magnesium.

2.2. Characterization

The synthesized samples were characterized by X-ray diffraction (XRD) using a Bruker D8 advanced X-ray diffractometer equipped with graphite-monochromatized Cu Ka radiation (λ = 1.5418 Å). Transmission electron microscopy (TEM) and high-resolution transmission electron microscope (HRTEM) images as well as selected area electron diffraction (SAED) pattern were recorded on a JEOL-2100 high-resolution transmission electron microscope at an acceleration voltage of 200 kV. Nitrogen sorption isotherm was performed at 77.3 K on a Tristar II 3020 M gas sorptometer. Raman spectroscopy was measured by a LABRAM-HR confocal laser MicroRaman spectrometer at an excitation wavelength of 514.5 nm.

2.3. Electrochemical measurements

The electrochemical properties of the samples were measured on a Land battery test system (CT2001A). To prepare the working electrode, a mixture of 70 wt% of active material (mesoporous Si nanorods, porous Si networks and bulk Si), 20 wt% of conducting acetylene black, and 10 wt% of sodium alginate in deionized water was pasted on a clean copper foil and then dried in vacuum at 60 °C for 10 h. The mass loading of the active material is about 0.9 mg cm^{-2}. The cell was fabricated by using lithium foil as the counter electrode, Celgard 2400 microporous polypropylene membrane as the separator, and the electrolyte consisted of a solution of 1 M $LiPF_6$ in a mixture of ethylene carbonate (EC) and dimethyl carbonate (DMC) (1: 1 v/v). The cell was assembled in an argon filled glovebox. Then, discharge and charge tests were carried out between 0.01 V and 3 V. Cycling performances were tested at a current density of 200 mA g^{-1}. Rate performances were measured at various current densities under the same conditions. Electrochemical impedance spectroscopy (EIS) was measured on an FRA-520 (MaterialsMates, Italia) connected to a Potentiostat-510 (MaterialsMates) over the frequency range of 100 kHz to 0.01 Hz with amplitude of 10 mV. All the electrochemical tests were carried out at 25 °C.

3. Results and Discussion

The preparation process of mesoporous silicon nanorods is shown in Fig. 1. First, the amorphous SiO_2 is grown on the MWCNTs via a simple sol-gel method at room temperature. Then, the composite of MWCNT/SiO_2 is annealed in air to remove the MWCNTs, leaving the SiO_2 nanotubes behind in the product. Finally, the SiO_2 nanotubes react with metallic Mg under Ar/H_2 atmosphere, producing mesoporous Si nanorods.

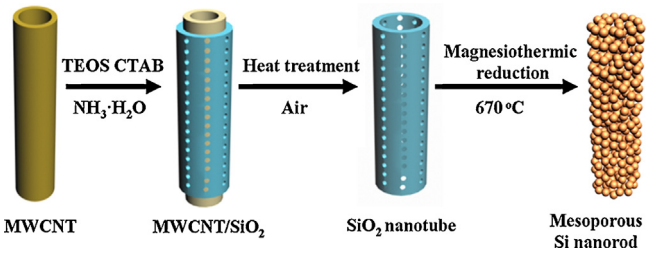

Fig. 1. Schematic illustration of the formation of obtained mesoporous silicon nanorods.

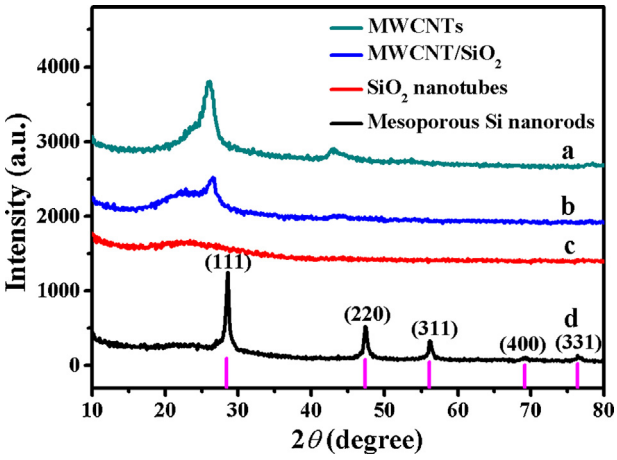

Fig. 2. XRD patterns of MWCNTs (a), MWCNT/SiO_2 composites (b), SiO_2 nanotubes (c) and as-prepared mesoporous silicon nanorods (d) (the magenta line at the bottom is the standard peak of silicon with a faced-centered cubic system).

Fig. 2 shows the XRD patterns of the products obtained at different stages of the preparation process. MWCNTs used as the template shows two pronounced peaks at 26° and 43°, as shown in Fig. 2a. After MWCNTs are coated by a silica layer, the corresponding peak intensities obviously decrease. Meanwhile, a broad peak between 20 and 25° appears in the pattern (Fig. 2b), which could be explained by the formation of amorphous silica [28]. Annealing the composite of MWCNT/SiO_2 in air effectively removes the MWCNTs, leaving amorphous SiO_2 behind in the product. This has

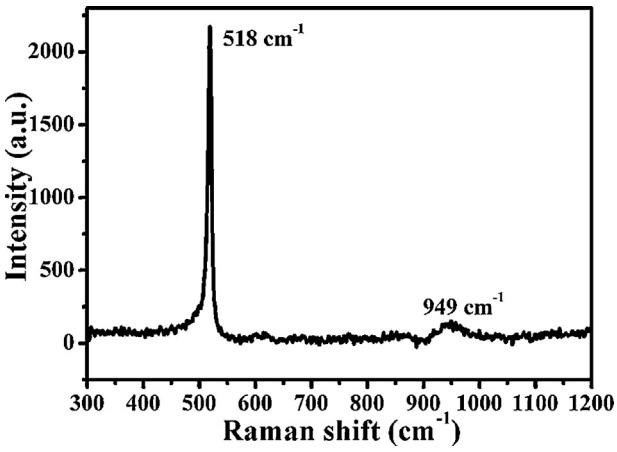

Fig. 3. Raman spectrum of as-prepared mesoporous silicon nanorods.

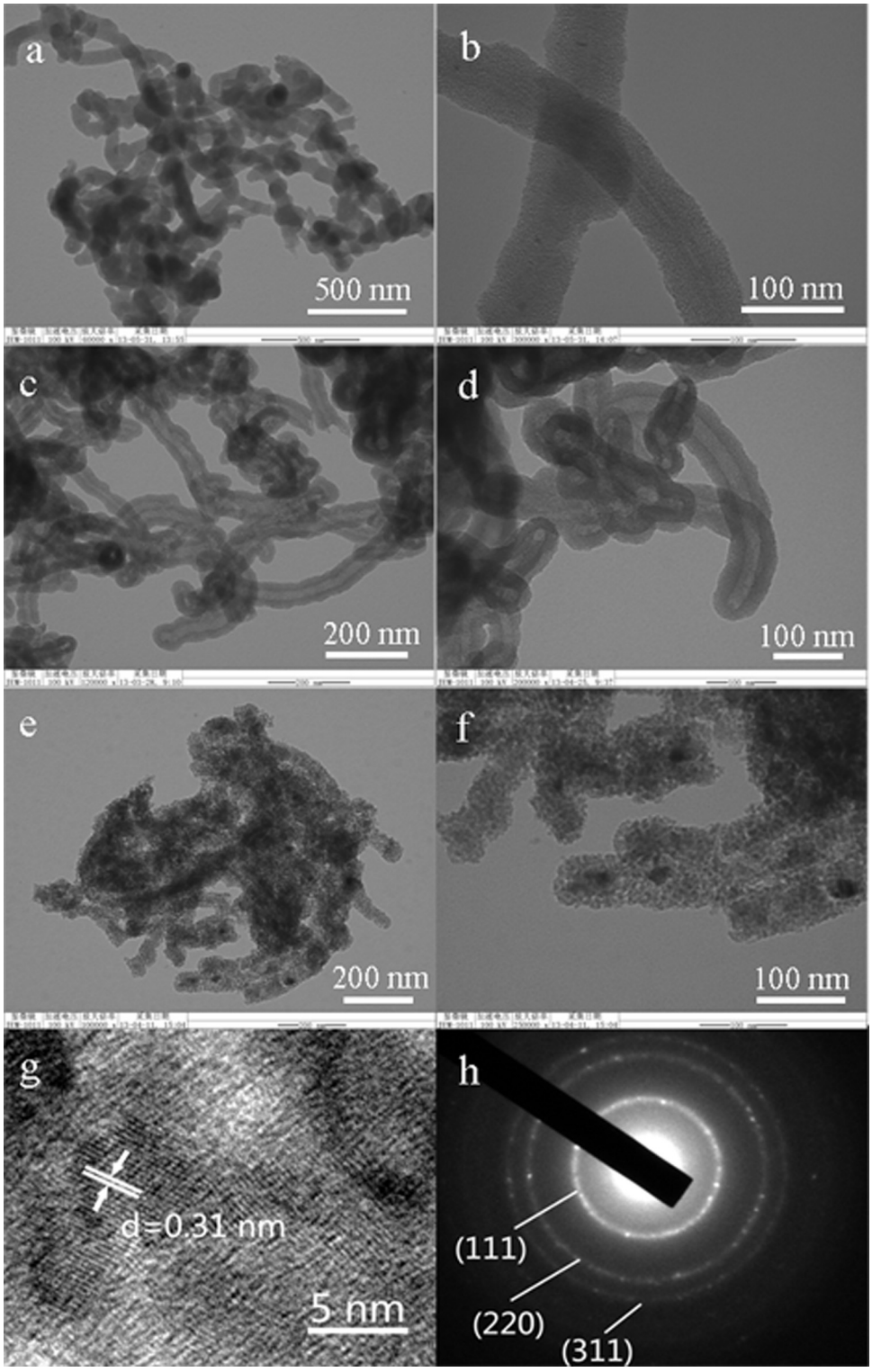

Fig. 4. TEM images of obtained MWCNT/SiO_2 composites (a) and (b), prepared SiO_2 nanotubes (c) and (d), obtained mesoporous silicon nanorods (e) and (f), High-resolution TEM image (g) and selected area Electron Diffraction Spectroscopy (SAED) (h).

been confirmed by the XRD pattern (Fig. 2c), where the peaks of MWCNTs completely disappear from the pattern after annealing. Reducing amorphous SiO_2 by Mg under Ar/H_2 atmosphere successfully produces crystalline silicon, as illustrated by Fig. 2d. All the diffraction peaks can be readily indexed to cubic phase silicon (JCPDS Card, No. 27-1402), suggesting the good crystallinity of silicon. Their average crystallite size is approximately 8 nm caculated by Scherrer Equation ($D = K\lambda/B\cos\theta$, where K is 0.89). The formation of silicon nanocrystals is attributed to the moderate reaction temperature and the inhibiting effect from *in-situ* synthesized magnesia [19]. It is noticed that there is a very weak peak over 20-25° in the pattern, suggesting a small amount of silica in the product [28]. This is also supported by the Raman spectrum (Fig. 3). Besides the sharp peak at 518 cm^{-1} from crystalline Si, the weak one at

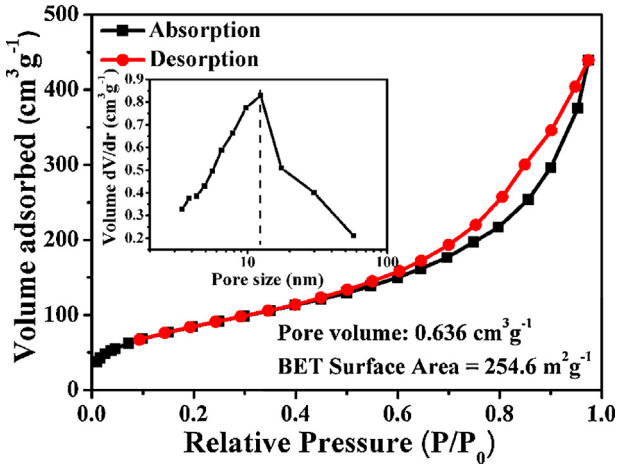

Fig. 5. Nitrogen adsorption-desorption isotherms of mesoporous silicon nanorods measured at 77.3 K (the inset is pore size distribution plot calculated by the BJH method).

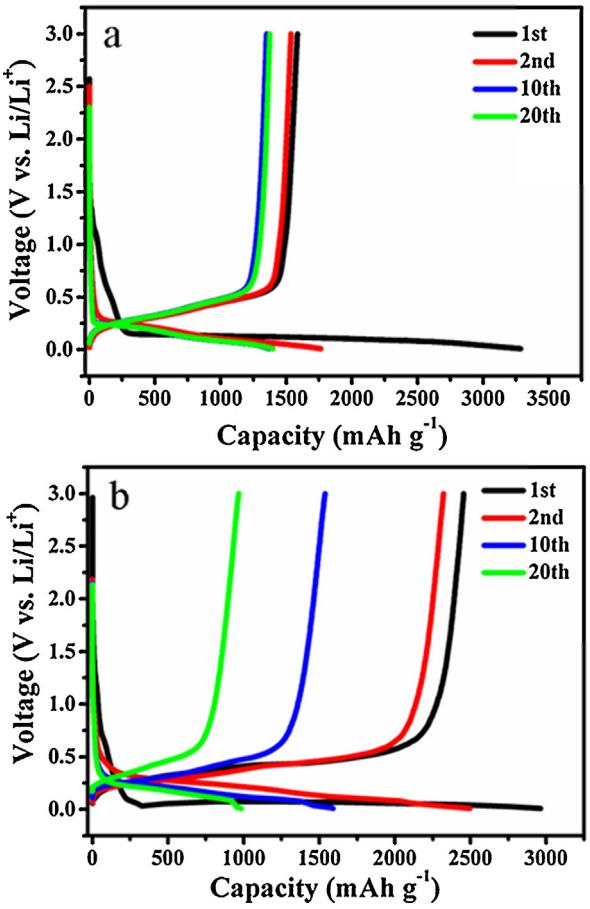

Fig. 6. Galvanostatic discharge-charge profiles of (a) mesoporous silicon nanorods and (b) porous silicon networks at the 1st, 2nd, 10th and 20th cycle, respectively.

949 cm^{-1} corresponds to amorphous SiO_2. The presence of amorphous SiO_2 in the product could be ascribed to unreacted species or surface oxidation of silicon.

Fig. 4 shows the TEM images of MWCNT/SiO_2, SiO_2 nanotubes and as-obtained mesoporous silicon nanorods. The composite of MWCNT/SiO_2 displays a typical one-dimensional feature inherited from MWCNTs (Fig. 4a). The close examination on the SiO_2 shell under high magnification reveals its porous structure (Fig. 4b), which could be attributed to the usage of CTAB in the sol-gel process [26,27]. After the removal of MWCNTs by a high-temperature annealing in air, the tubular characteristics can be easily observed in the product (Fig. 4c). Meanwhile, the mesoporous structure is still kept in the wall of the SiO_2 nanotubes (Fig. 4d). The wall thickness of the nanotubes is around 23 nm. The reaction of the porous SiO_2 nanotubes with Mg resulted in the structure destruction and then the formation of the mesoporous nanorods, as shown in Fig. 4e. Fig. 4f clearly reveals the aggregation of small nanoparticles into the mesoporous nanorods. The HRTEM image shows interplanar distances about 0.31 nm (Fig. 4g), corresponding to (111) plane of crystalline silicon. The electron diffraction pattern comprises several bright concentric rings (Fig. 4h), indicating the polycrystalline nature of the mesoporous nanorods. The diffraction rings can be identified as the reflections from the crystal planes of (111), (220) and (311) of cubic-phase silicon.

The nitrogen adsorption-desorption measurement was carried out to determine the surface area and the pore-related information of the mesoporous silicon nanorods. As described in Fig. 5, a distinct hysteretic loop for P/P_0 ranges from 0.5 to 1.0 can be observed, suggesting the presence of pores in the product. Based on the BJH method, an average pore size is estimated to be about 12 nm. The pore volume and surface area of the mesoporous silicon nanorods are 0.636 $cm^3\ g^{-1}$ and 254.6 $m^2\ g^{-1}$, respectively. The large specific surface area and porous structure of the mesoporous silicon nanorods provide better penetration of electrolyte and the possibility of the efficient transport of electrons and lithium ions [29].

The electrochemical properties of the mesoporous silicon nanorods as an anode are shown in Fig. 6. As presented in Fig. 6a, the discharge and charge curves of the mesoporous nanorods were measured over the voltage range 0.01 V to 3 V at a current density of 200 mA g^{-1} for 1st, 2nd, 10th and 20th cycles. There are three plateaus in the first discharge curve. The very small plateaus at 1.2 and 0.8 V are mainly attributed to the decomposition of organic electrolyte and the formation of solid electrolyte interface (SEI) film on the electrode surface. The long and flat plateau at 0.1 V could be ascribed to the lithiation process of crystalline Si to amorphous Li_xSi phase [30,31]. The first discharge capacity of the mesoporous nanorods is as high as 3285 mAh g^{-1}, and the subsequent charge gives a capacity of 1586 mAh g^{-1}, corresponding to a high irreversible capacity, which is attributed to the existence of a small amount of amorphous SiO_2, decomposition of organic electrolyte and formation of SEI film. The discharge capacity for the second cycle is about 1765 mAh g^{-1} with a coulombic efficiency of 87.1%. After 20 cycles, the discharge and charge capacities are 1398 and 1376 mAh g^{-1}, respectively. The coulombic efficiency reaches as high as 98.4%. The lithium storage performance of the mesoporous nanorods is much better than that of the porous Si networks (Fig. S1 and S2), as shown in Fig. 6b. Although the first discharge and charge capacities of the porous networks are 2963 and 2455 mAh g^{-1}, both of them decay quickly during the cycling process. After 20 cycles, the discharge and charge capacities step down to 983 and 967 mAh g^{-1}, much lower than those of the mesoporous silicon nanorods. The rapid decreasing might be associated with the big size of the networks, which easily leads to the pulverization of the electrode and the loss of the active materials.

The cycling performances of the mesoporous nanorods and the porous networks are shown in Fig. 7. The reversible capacity of the mesoporous silicon nanorods is 1038 mAh g^{-1} at a current density of 200 mA g^{-1} after 170 cycles (Fig. 7a). Nevertheless, the reversible capacity of the porous networks is only 501.5 mAh g^{-1} after the same cycles (Fig. 7b), showing the improved cycling stability of the mesoporous nanorods. Although the cycling stability of the porous networks is poor in comparison with that of the mesoporous

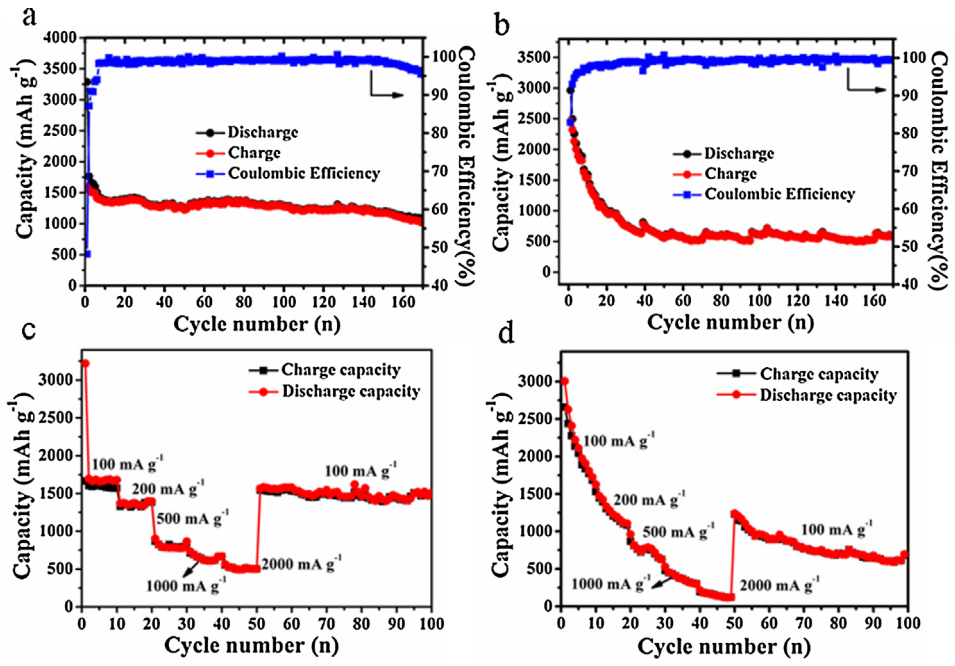

Fig. 7. (a) and (b) Cycling performances and coulomb efficiencies of as-prepared mesoporous silicon nanorods and porous silicon networks at a current density of 200 mA g^{-1} after 170 cycles. (c) and (d) Rate performances of as-prepared mesoporous silicon nanorods and porous silicon networks at different current densities from 100 to 2000 mA g^{-1}.

nanorods, it is still better than that of bulk silicon (Fig. S3). The high cycling stability of the mesoporous nanorods is attributed to their mesoporous feature and nanoscale size, which can tolerate the volume expansion during the discharge and charge processes.

Fig. 7c and d display the rate performances of the mesoporous nanorods and the porous networks at different current densities. When the current density is 100, 500, or 2000 mA g^{-1}, the corresponding reversible capacity of the mesoporous nanorods is 1603, 866 or 664 mAh g^{-1}, respectively. The data are much higher than those of the porous networks. At a rate of 2000 mA g^{-1}, the reversible capacity of the porous networks is only 299 mAh g^{-1}. Even after the current density rebounds to 100 mA g^{-1}, the reversible capacity only recovers to 681 mAh g^{-1} after 100 cycles, which is still lower than that of the mesoporous nanorods at 1545 mAh g^{-1}. This confirms the superior performances of the mesoporous nanorods in lithium storage.

On the basis of the above results, the high specific capacity, good cycling and rate performances of the mesoporous nanorods could be explained by their nanoscale size and porous structure. Nanoscale size leads to reduced diffusion lengths for Li^+ and electron transport to the current collector [32]. Porous structure can alleviate the large volume expansion of silicon and thus maintain the structure stability during the cycling process [33–36]. As a result of nanoscale size and porous structure, high specific surface area promotes the contact between the electrode and the electrolyte, benefiting the transportation and storage of lithium at the interface, although it also increases the irreversible capacity for the first cycle.

EIS spectra of the mesoporous silicon nanorods and porous silicon networks after various cycles charging to 3 V are shown in Fig. 8. The big semicircle from the high frequency to medium frequency region represents the SEI film resistance (or contact resistance) and the charge transfer resistance on the interface of the electrode and the electrolyte. Besides, the straight sloped line in the low frequency region corresponds to the lithium diffusion resistance inside the electrode [37,38]. It is noted that the impedance undergo a gradually decreasing process in the first five cycles for

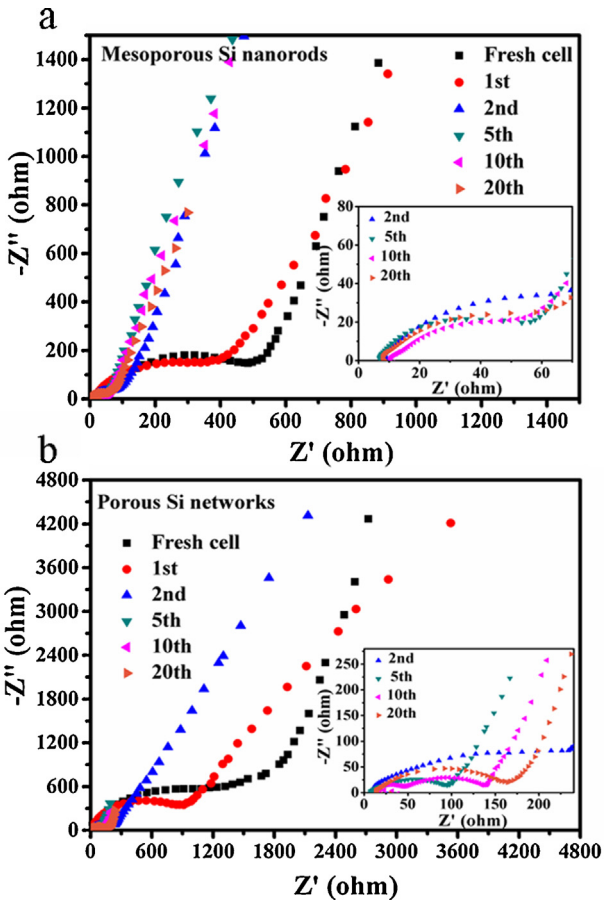

Fig. 8. Nyquist plots of the mesoporous silicon nanorods (a) and porous silicon networks (b) after charging to 3 V in a series of cycles (the inset is the magnified Nyquist plots for both electrodes).

both half cells. Afterwards, both of the resistances increase to some degree from the tenth cycle (Fig. 8a and b). This phenomenon might be explained as follows: The surface of the Si electrode is initially covered with a nonconducting native layer consisting of silicon oxide and silanol [39,40]. After that, when the surface of silicon electrode is covered with the initial SEI layer, the total resistance is abruptly decreased to a minimum value. This observation is also in consistent with the previous reports [40,41]. Moreover, the total resistance for mesoporous silicon nanorods in any cycle is distinctly smaller than that of porous silicon networks. As the cycle number increases, the total resistance for the porous silicon networks increases faster than that of the mesoporous silicon nanorods (from 5th to 20th cycle). This trend is in good accordance with the electrochemical performance of both electrodes.

4. Conclusions

In summary, novel mesoporous silicon nanorods have been prepared using MWCNTs as a template via a facile magnesiothermic reduction method. When evaluated as anode materials in LIBs, high specific capacity, good cycling performance and rate capability could be obtained. Compared with the porous silicon networks and bulk silicon, the reversible capacity can retain as high as 1038 mAh g^{-1} after 170 cycles. Even at a high current density of 2000 mA g^{-1}, the reversible capacity of 664 mAh g^{-1} can still be achieved. This new silicon nanostructure and facile preparation methods coupled with good electrochemical performance provide the possibility to be used in large scale as an anode material for LIBs.

Acknowledgements

This work was supported by the 973 Project of China (No. 2011CB935901), the National Nature Science Foundations of China (No. 91022033, 21203111, 21071055, and 51172076), New Century Excellent Talents in University (NCET-10-0369), Shandong Provincial Natural Science Foundation for Distinguished Young Scholar (JQ201205), Independent Innovation Foundations of Shandong University (2012ZD007), and new-faculty start-up funding in Shandong University.

Appendix A. Supplementary data

Supplementary data associated with this article can be found, in the online version, at http://dx.doi.org/10.1016/j.electacta.2014.01.158.

References

[1] M. Armand, J.-M. Tarascon, Building better batteries, Nature 451 (2008) 652.
[2] M. Winter, J.O. Besenhard, M.E. Spahr, P. Novak, Insertion electrode materials for rechargeable lithium batteries, Advanced Materials 10 (1998) 725.
[3] B.A. Boukamp, G.C. Lesh, R.A. Huggins, All-Solid Lithium Electrodes with Mixed-Conductor Matrix, Journal of the Electrochemical Society 128 (1981) 725.
[4] C.K. Chan, H. Peng, G. Liu, K. McIlwrath, X.F. Zhang, R.A. Huggins, Y. Cui, High-performance lithium battery anodes using silicon nanowires, Nature Nanotechnology 3 (2008) 31.
[5] C.K. Chan, R.N. Patel, M.J. O'Connell, B.A. Korgel, Y. Cui, Solution-Grown Silicon Nanowires for Lithium-Ion Battery Anodes, ACS Nano 4 (2010) 1443.
[6] M. Ge, J. Rong, X. Fang, C. Zhou, Porous Doped Silicon Nanowires for Lithium Ion Battery Anode with Long Cycle Life, Nano Letters 12 (2012) 2318.
[7] J.P. Maranchi, A.F. Hepp, P.N. Kumta, High Capacity, Reversible Silicon Thin-Film Anodes for Lithium-Ion Batteries, Electrochemical and Solid-State Letters 6 (2003) A198.
[8] M.K. Datta, J. Maranchi, S.J. Chung, R. Epur, K. Kadakia, P. Jampani, P.N. Kumta, Amorphous silicon-carbon based nano-scale thin film anode materials for lithium ion batteries, Electrochimica Acta 56 (2011) 4717.
[9] Y.Y. Tang, X.H. Xia, Y.X. Yu, S.J. Shi, J. Chen, Y.Q. Zhang, J.P. Tu, Cobalt nanomountain array supported silicon film anode for high-performance lithium ion batteries, Electrochimica Acta 88 (2013) 664.
[10] Y. Yao, M.T. McDowell, I. Ryu, H. Wu, N. Liu, L. Hu, W.D. Nix, Y. Cui, Interconnected Silicon Hollow Nanospheres for Lithium-Ion Battery Anodes with Long Cycle Life, Nano Letters 11 (2011) 2949.
[11] H. Ma, F. Cheng, J.-Y. Chen, J-Z. Zhao, C-S. Li, Z-L. Tao, J. Liang, Nest-like Silicon Nanospheres for High-Capacity Lithium Storage, Advanced Materials 19 (2007) 4067.
[12] X. Zhou, J. Tang, J. Yang, J. Xie, L. Ma, Silicon@carbon hollow core-shell heterostructures novel anode materials for lithium ion batteries, Electrochimica Acta 87 (2013) 663.
[13] T. Song, J. Xia, J.-H. Lee, D.H. Lee, M.-S. Kwon, J.-M. Choi, J. Wu, S.K. Doo, H. Chang, W.I. Park, D.S. Zang, H. Kim, Y. Huang, K.-C. Hwang, J.A. Rogers, U. Paik, Arrays of Sealed Silicon Nanotubes As Anodes for Lithium Ion Batteries, Nano Letters 10 (2010) 1710.
[14] M.-H. Park, M.G. Kim, J. Joo, K. Kim, J. Kim, S. Ahn, Y. Cui, J. Cho, Silicon Nanotube Battery Anodes, Nano Letters 9 (2009) 3844.
[15] J. Jiang, Y. Li, J. Liu, X. Huang, Building one-dimensional oxide nanostructure arrays on conductive metal substrates for lithium-ion battery anodes, Nanoscale 3 (2011) 45.
[16] P.L. Taberna, S. Mitra, P. Poizot, P. Simon, J.-M. Tarascon, High rate capabilities Fe_3O_4-based Cu nano-architectured electrodes for lithium-ion battery applications, Nature Materials 5 (2006) 567.
[17] L.-F. Cui, Y. Yang, C.-M. Hsu, Y. Cui, Carbon-Silicon Core-Shell Nanowires as High Capacity Electrode for Lithium Ion Batteries, Nano Letters 9 (2009) 3370.
[18] L.-F. Cui, R. Ruffo, C.K. Chan, H. Peng, Y. Cui, Crystalline-Amorphous Core-Shell Silicon Nanowires for High Capacity and High Current Battery Electrodes, Nano Letters 9 (2009) 491.
[19] Z. Bao, M.R. Weatherspoon, S. Shian, Y. Cai, P.D. Graham, S.M. Allan, G. Ahmad, M.B. Dickerson, B.C. Church, Z. Kang, H.W. Abernathy III, C.J. Summers, M. Liu, K.H. Sandhage, Chemical reduction of three-dimensional silica microassemblies into microporous silicon replicas, Nature 446 (2007) 172.
[20] Y. Yu, L. Gu, C. Zhu, S. Tsukimoto, P.A. Aken, J. Maier, Reversible Storage of Lithium in Silver-Coated Three-Dimensional Macroporous Silicon, Advanced Materials 22 (2010) 2247.
[21] H. Jia, P. Gao, J. Yang, J. Wang, Y. Nuli, Z. Yang, Novel Three-Dimensional Mesoporous Silicon for High Power Lithium-Ion Battery Anode Material, Advanced Energy Materials 1 (2011) 1036.
[22] A. Xing, S. Tian, H. Tang, D. Losic, Z. Bao, Mesoporous silicon engineered by reduction of biosilica from rice husk as high-performance anode for lithium-ion batteries, (Communication) RSC Advances 3 (2013) 10145.
[23] W. Chen, Z. Fan, A. Dhanabalan, C. Chen, C. Wang, Mesoporous Silicon Anodes Prepared by Magnesiothermic Reduction for Lithium Ion Batteries, Journal of the Electrochemical Society 158 (2011) A1055.
[24] J. Chen, L. Yang, S. Rousidan, S. Fang, Z. Zhang, S. Hirano, Facile fabrication of Si mesoporous nanowires for high-capacity and long-life lithium storage, Nanoscale 5 (2013) 10623.
[25] Y.K. Yang, X.L. Xie, J.G. Wu, Z.F. Yang, X.T. Wang, Y.W. Mai, Multiwalled Carbon Nanotubes Functionalized by Hyperbranched Poly(urea-urethane)s by a One-Pot Polycondensation, Macromolecular Rapid Communications 27 (2006) 1695.
[26] K.L. Ding, B.J. Hu, Y. Xie, G.M. An, R.T. Tao, H.Y. Zhang, Z.M. Liu, A simple route to coat mesoporous SiO_2 layer on carbon nanotubes, Journal of Materials Chemistry 19 (2009) 3725.
[27] M. Zhang, Y. Wu, X. Feng, X. He, L. Chen, Y. Zhang, Fabrication of mesoporous silica-coated CNTs and application in size-selective protein separation, Journal of Materials Chemistry 20 (2010) 5835.
[28] P. Lu, Y.-L. Hsieh, Highly pure amorphous silica nano-disks from rice straw, Powder Technology 225 (2012) 149.
[29] Y. Xia, W. Zhang, Z. Xiao, H. Huang, H. Zeng, X. Chen, F. Chen, Y. Gan, X. Tao, Biotemplated fabrication of hierarchically porous NiO/C composite from lotus pollen grains for lithium-ion batteries, Journal of Materials Chemistry 22 (2012) 9209.
[30] S.R. Gowda, V. Pushparaj, S. Herle, G. Girishkumar, J.G. Gordon, H. Gullapalli, X. Zhan, P.M. Ajayan, A.L.M. Reddy, Three-Dimensionally Engineered Porous Silicon Electrodes for Li Ion Batteries, Nano Letter 12 (2012) 6060.
[31] Y. Yang, J.-G. Ren, X. Wang, Y.-S. Chui, Q.-H. Wu, X. Chen, W. Zhang, Graphene encapsulated and SiC reinforced silicon nanowires as an anode material for lithium ion batteries, Nanoscale 5 (2013) 8689.
[32] Y.-M. Lin, P.R. Abel, A. Heller, C. Buddie Mullins, α-Fe_2O_3 Nanorods as Anode Material for Lithium Ion Batteries, Journal of Physical Chemistry Letters 2 (2011) 2885.
[33] E. Kim, D. Son, T.-G. Kim, J. Cho, B. Park, K.-S. Ryu, S.-H. Chang, A Mesoporous/Crystalline Composite Material Containing Tin Phosphate for Use as the Anode in Lithium-Ion Batteries, Angewandte Chemie 116 (2004) 6113.
[34] S.-J. Bao, Q.-L. Bao, C.-M. Li, Z.-L. Dong, Novel porous anatase TiO_2 nanorods and their high lithium electroactivity, Electrochemistry Communications 9 (2007) 1233.
[35] R. Demir-Cakan, Y.S. Hu, M. Antonietti, J. Maier, M.M. Titirici, Facile One-Pot Synthesis of Mesoporous SnO_2 Microspheres via Nanoparticles Assembly and Lithium Storage Properties, Chemistry of Materials 20 (2008) 1227.
[36] W. Luo, X. Hu, Y. Sun, Y. Huang, Electrospun porous $ZnCo_2O_4$ nanotubes as a high-performance anode material for lithium-ion batteries, Journal of Materials Chemistry 22 (2012) 8916.

[37] S.-L. Chou, J.-Z. Wang, M. Choucair, H.-K. Liu, J.A. Stride, S.-X. Dou, Enhanced reversible lithium storage in a nanosize silicon/graphene composite, Electrochemistry Communications 12 (2010) 303.
[38] S. Yang, H. Song, H. Yi, W. Liu, H. Zhang, X. Chen, Carbon nanotube capsules encapsulating SnO_2 nanoparticles as an anode material for lithium ion batteries, Electrochimica Acta 55 (2009) 521.
[39] M. Yoshio, H. Wang, K. Fukuda, T. Umeno, N. Dimov, Z. Ogumi, Carbon-Coated, Si as a Lithium-Ion Battery Anode Material, Journal of the Electrochemical Society 149 (2002) A1598.
[40] Y.M. Lee, J.Y. Lee, H.-T. Shim, J.K. Lee, J.-K. Park, SEI Layer Formation on Amorphous Si Thin Electrode during Precycling, Journal of the Electrochemical Society 154 (2007) A515.
[41] Y. Zhao, X. Liu, H. Li, T. Zhai, H. Zhou, Hierarchical Micro/Nano Porous Silicon Li-ion Battery Anode, good electrochemical performance of the mesoporous silicon nanorods anode, Chemical Communications 48 (2012) 5079.